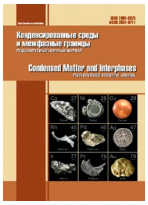

ISSN 1606-867X (Print)
ISSN 2687-0711 (Online)
Condensed Matter and Interphases
Kondensirovannye Sredy i Mezhfaznye Granitsy
https://journals.vsu.ru/kcmf/

Original articles

Research article
https://doi.org/10.17308/kcmf.2025.27/12488

Chemical vapor deposition of $Tm_3Fe_5O_{12}$ epitaxial films, investigation of their structure and properties in the terahertz range

M. N. Markelova✉, A. A. Hafizov, Shi Xiaoyu, I. E. Graboy, M. S. Shanin, M. R. Konnikova, A. P. Shkurinov, A.R. Kaul

[1]*Lomonosov Moscow State University,*
1 Leninskie Gory, Moscow 119991, Russian Federation

Abstract

In this study, for the search and development of new spintronic materials, thin films of $Tm_3Fe_5O_{12}$ iron garnet were obtained by the metalorganic chemical vapor deposition (MOCVD) on single-crystal $Gd_3Ga_5O_{12}$(111) – GGG and $Y_3Al_5O_{12}$(111) – YAG substrates. The $Tm_3Fe_5O_{12}$ films were investigated using X-ray diffraction, Energy dispersive X-Ray microanalysis, Raman spectroscopy and terahertz (THz) pulsed spectroscopy.

The epitaxial nature of films deposited on substrates of both types demonstrated. It was found that the growth of garnet film under the high-temperature vacuum conditions of MOCVD on a GGG substrate is complicated by the evaporation of gallium oxide, which causes the introduction of iron oxide into the surface layer of the substrate, enrichment of the adjacent layer of the film with thulium oxide and the formation of non-stoichiometric garnet with antisite defects.

It was concluded that YAG substrates are more promising, since the heteroepitaxy of iron garnets on them does not have such complications.

Keywords: Thin films, Iron garnets, MOCVD, Structure, Antisite defects, Raman spectroscopy, Terahertz spectroscopy

Funding: Work on MOCVD film production was carried out using equipment purchased using funds from the Moscow University Development Program. The study was carried out with the financial support of the Interdisciplinary Scientific and Educational Schools of Moscow University (Project No. 24-Ш06-13).

For citation: Markelova M. N., Hafizov A. A., Shi X., Graboy I. E., Shanin M. S., Konnikova M. R., Shkurinov A. P., Kaul A. R. Chemical vapor deposition of $Tm_3Fe_5O_{12}$ epitaxial films, investigation of their structure and properties in the terahertz range. *Condensed Matter and Interphases*. 2025;27(1): 104–114. https://doi.org/10.17308/kcmf.2025.27/12488

Для цитирования: Маркелова М. Н., Хафизов А. А., Ши С., Грабой И. Э., Шанин М. С., Конникова М. Р., Шкуринов А. П., Кауль А. Р. Химическое газофазное осаждение эпитаксиальных пленок $Tm_3Fe_5O_{12}$, исследование их структуры и свойств в терагерцовом диапазоне. *Конденсированные среды и межфазные границы*. 2025;27(1): 104–114. https://doi.org/10.17308/kcmf.2025.27/12488

✉ Maria N. Markelova, e-mail: maria.markelova@gmail.com

1. Introduction

The successes achieved in the last decade in the development of new areas of electronics – spintronics and magnonics are based on the development and application of new materials, including those combining several functional properties [1]. One of the main trends in modern engineering is the miniaturization of electronic devices, so research and development of multifunctional materials in the form of thin films is of particular interest. This direction of development is especially relevant for spintronics and magnonics, which use ferrimagnets with a garnet structure in the form of ultra-thin (from units to tens of nanometers) epitaxial films as the main materials [1]. To obtain such thin films, the liquid-phase epitaxy method, which has long been the most popular method for synthesizing garnets (the thickness of the films obtained in this case is a few micrometers [2, 3]), cannot be used; therefore, new technological approaches to obtaining thin films of iron garnets are required. One of the promising synthesis methods is the metalorganic chemical vapor deposition (MOCVD) using , which has become the main method in the synthesis of epitaxial heterostructures of semiconductors [4]. Using b-diketonates and alcoholates as volatile substances, MOCVD can also be quite successfully applied to the epitaxy of functional materials based on simple and complex oxides [5].

The structural class of garnets belongs to the space group *Ia*3*d*. The cubic body-centered unit cell of garnet contains 8 identical octants corresponding to the formula composition $\{RE\}_3[Fe]_2(Fe)_3O_{12}$, where the curly brackets { } denote the dodecahedral positions of the rare earth element (RE), and the brackets [ ]- and ( )- correspond to the octahedral and tetrahedral positions occupied by Fe^{3+} ions. Thus, the features of iron-based garnets are: a multi-sublattice magnetic structure, have wide possibilities for varying the elemental composition and, as a consequence, a variety of their magnetic properties [6].

Iron garnets of rare earth elements (REE) have high resistance and, accordingly, high transparency in the visible and near IR ranges, which gives them an advantage over metallic ferromagnets (Fe, Ni, etc.), since it allows the use of the pump-probe technique in the study of ultra-fast magnetization dynamics [1,7]. Spin pumping is also a way to excite magnons in magnetic systems. Recently, spin wave propagation in a lutetium iron garnet/heavy metal ($Lu_3Fe_5O_{12}$/Pt) is demonstrated in [8]. The results of such studies, along with great fundamental interest, open up prospects for the creation of ultra-high-speed devices for recording and processing information using thin ferrimagnetic films [9].

Spin-flip transitions of some rare earth iron garnets occur in the frequency range from 0.1 THz to 10 THz. Therefore, terahertz radiation can potentially affect the spin state of such systems and can be used to obtain important results in the study of magnetic dynamics under the influence of laser radiation [10], however, research in this direction is in the initial phase of its development. Systematic studies of the spectral properties of iron garnet films in the THz range and their changes in a number of rare earth elements are of great interest.

Thus, the aim of this study was the MOCVD synthesis of thin films of $Tm_3Fe_5O_{12}$ iron garnet, comparative analysis of the results of epitaxy on isomorphic $Gd_3Ga_5O_{12}$ and $Y_3Al_5O_{12}$ (111) substrates, investigation of the structure of the obtained films by X-ray diffraction, Raman spectroscopy, and also study of their spectral characteristics by time-resolved pulsed THz spectroscopy.

2. Experimental

Thin $Tm_3Fe_5O_{12}$ films were synthesized on single-crystal $Ga_3Ga_5O_{12}$ (GGG) and $Y_3Al_5O_{12}$ (YAG) substrates with the (111) orientation by metal-organic chemical vapor deposition (MOCVD). Dipivaloylmethanates $Tm(thd)_3$ and $Fe(thd)_3$ (thd – 2,2,6,6-tetramethylheptane-3,5-dionate anion) were used as volatile compounds (precursors). In our previous study, we discussed in detail a new principle of dosing precursor vapor into the reactor, which ensures smooth, well-controlled and reproducible "feeding" of the growing film [11]. The scheme of the modernized setup using this principle and applied in this study is shown in Fig. 1. The system operates by passing a cotton thread impregnated with an metalorganic precursor solution through two separate vacuum zones – a low-temperature solvent evaporation

zone and a higher-temperature zone where precursors sublimate. The solvent vapors (toluene was used) are condensed in a nitrogen trap, and the precursor vapors are transferred by a carrier gas flow (Ar) into a vertical hot-wall reactor, where their oxidative thermolysis occurs with the formation of an oxide film on a heated substrate. The substrate holder with the substrate fixed to it rotates around a vertical axis in order to increase the lateral homogeneity of the films by thickness. The vacuum in the system is created by a fore vacuum pump equipped with a valve for regulating the overall pressure in the film deposition zone. The temperature of the hot lines through which the precursor vapors are supplied and the temperature of the substrate holder were 190 and 910 °C respectively; the total pressure was 10 mbar, the partial pressure of oxygen was 1 mbar, the film growth rate was 3 nm/min. After film deposition, the setup was filled with oxygen to atmospheric pressure and oxidative annealing was carried out at the spraying temperature for 20 min, after which the setup was cooled. The thickness of the films was 900 nm.

The Fe/Tm ratio in the obtained films was determined by Energy dispersive X-Ray microanalysis (EDX) data using a Zeiss EVO 50 SEM scanning electron microscope with an e2v Sirius SD EDX analyzer. The phase composition and orientation of the obtained films were determined based on X-ray θ-2θ scanning data using a Rigaku SmartLab diffractometer (Cu$K\alpha$, graphite monochromator). Measurement in the θ-2θ scanning mode was carried out in the angle range of 5–80° with a step of 0.02°, the signal accumulation time was 1 s. Phase analysis was performed using the ICDD PDF database. For the determination of the in-plane orientation of the films and confirm epitaxial growth, X-ray ϕ-scanning was performed.

Raman spectra at wavelengths of 532 and 785 nm were obtained using a HORIBA Scientific Raman spectrometer and microscope. The measurement range was from 80 to 2000 cm^{-1}. Raman spectroscopy was performed with a 100x objective at an incident radiation intensity of 140 W/cm^2 for λ = 532 nm and $3.6 \cdot 10^3$ W/cm^2 for λ = 785 nm. Three independent measurements were performed, each of which was averaged over 30 scans with an accumulation time of 0.5 s at each point. The background component of the spectrum was subtracted using the Voight

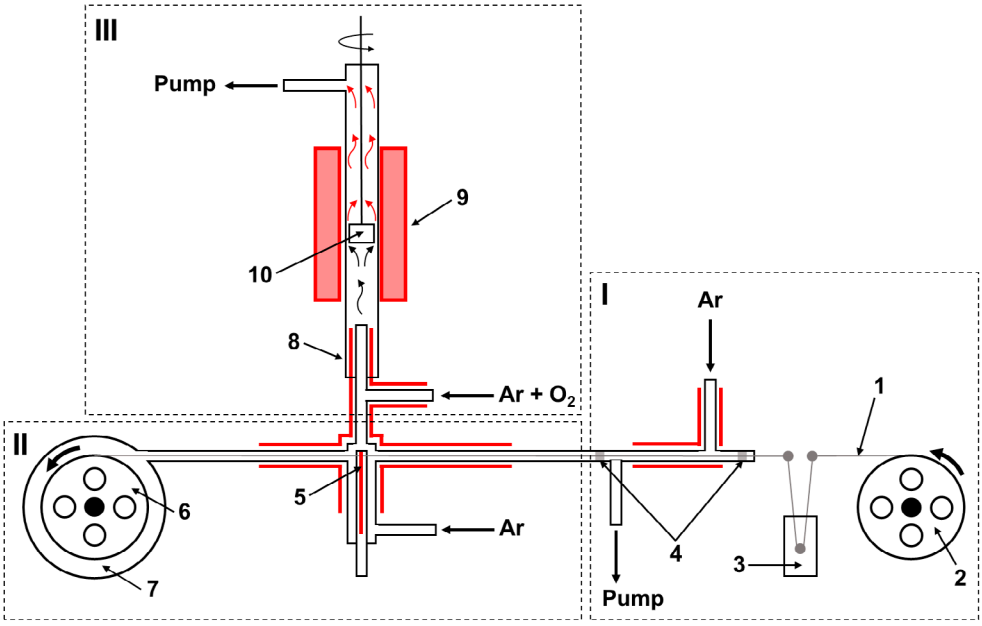

Fig. 1. Schematic diagram of MOCVD setup with thread-solution feeder. **I** – Thread feeding and solvent evaporation unit: *1* – cotton thread, *2* – feeding reel, *3* – reservoir for precursor solution, *4* – dies. **II** – Precursor evaporation unit: *5* – precursor evaporator, *6* – receiving reel, *7* – vacuum cover of the receiving reel. **III** – Film deposition unit: *8* – quartz reactor, *9* – reactor furnace, *10* – rotating substrate holder. Heated lines are marked in red

function approximation of the obtained Raman spectra.

Terahertz spectroscopy in both transmission and reflection geometry was performed using a commercial TeraSmart THz spectrometer (Menlo Systems GmbH, Germany). Linear p-polarized THz pulses are generated in a fiber-coupled photoconductive antenna (Fe:InGaAs/INASAS) and measured by two photoconductive detectors (LT InGaAs/InAlAs), which simultaneously measure the transmitted and reflected THz beams. The spectrometer has a dynamic range of 95 dB, a spectral range of 0.2–3.6 THz and a scan window of 110 ps, providing a frequency resolution of 7.3 GHz. The spectral range for measurements is limited in the low-frequency region by the sample aperture (4 mm), and in the high-frequency region (above 3.6 THz) by the detectors' absorption lines. The THz radiation was focused onto the sample by two parabolic mirrors, and the THz beam size on the sample was about 500 μm at the $1/e^2$ level. In this study, the incidence angle was 35°. To reduce the effect of water vapor absorption, the experiments were conducted using a dry air system that maintained a relative humidity of 20% in the chamber. In addition, to reduce systematic error, 3 independent measurements of 1000 pulses each were performed for each sample, the results of which were averaged.

The method for obtaining the absorption coefficient and refractive index for the transmission configuration is described in [12,13]. Determination of the dependence of the amplitude of the transmitted field on the frequency (w) is possible using the Fourier transforms (FFT) of the time profile of the THz pulse $E(t)$:

$$E_{\text{sample}}(\omega) = FFT\left(E(t)\right). \quad (1)$$

The transmittance coefficient $T_w(\omega)$ of the sample is calculated as the ratio of the amplitude of the field passed through the sample to the amplitude of the field without the sample (air):

$$T_w(\omega) = \frac{\text{substrate}(\omega)}{E_{\text{air}}(\omega)}. \quad (2)$$

From here the absorption index of the sample is calculated as:

$$\alpha(\omega) = \frac{-\ln\left(T_w(\omega)\right) + \ln(1-R^2)}{d}, \quad (3)$$

$$n(\omega) = n_{\text{aver}} + \arg(T_w(\omega))\frac{c}{\omega d}, \quad (4)$$

where d – sample thickness, $R = \frac{n_{\text{aver}}-1}{n_{\text{aver}}+1}$ – reflection coefficient, $n_{\text{aver}} = 1 + \Delta t \cdot \frac{c}{d}$ – average refractive index, Δt – pulse delay when passing through the sample, c – the speed of light.

3. Results and discussion

For deposition of $Tm_3Fe_5O_{12}$ films two substrates with a garnet structure were selected – GGG(111) and YAG(111) with very different unit cell parameters (Fig. 2), which leads to different values of the unit cell parameter mismatch (e) at the film/substrate interface. Values e, calculated using the formula:

$$\varepsilon = \frac{a_{\text{substrate}} - a_{\text{film}}}{a_{\text{substrate}}} \cdot 100\ \%, \quad (5)$$

were 0.4% and -2.8% for films on GGG(111) and YAG(111), respectively. As can be seen from the calculated values, during epitaxy on YAG, the substrate compresses the film in-plane, and in the case of GGG, on the contrary, the substrate stretches the film in-plane. Thus, during the growth of $Tm_3Fe_5O_{12}$ films on these substrates, significant elastic stresses can be expected in the films, which usually lead to changes in many physical properties, in particular magnetic ones.

The θ/2θ diffraction patterns of $Tm_3Fe_5O_{12}$ films, obtained by simultaneous deposition on GGG(111) and YAG(111) substrates are shown

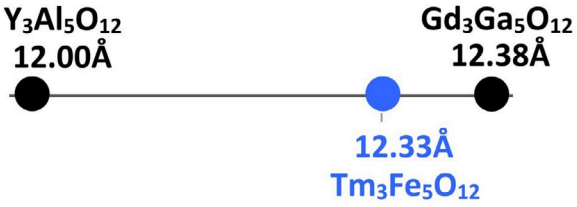

Fig. 2. Schematic illustration of the difference in the unit cell parameters of $Gd_3Ga_5O_{12}$(111) and $Y_3Al_5O_{12}$(111) garnet substrates and $Tm_3Fe_5O_{12}$ film

in Fig. 3a. It is evident that in both diffraction patterns, in addition to the substrate peaks, there were peaks from the $Tm_3Fe_5O_{12}$ film (444), however, on the GGG(111) substrate there were also additional peaks, designated **2** and **3** (Fig. 3a, b). This result is identical to recently observed in our study of the structure of lutetium iron garnet $Lu_3Fe_5O_{12}$ films on GGG substrates [14]. Under MOCVD synthesis conditions ($T_{deposition}$ = 890-950 °C and low partial pressure of oxygen ~1 mbar) surface chemical instability of the $Gd_3Ga_5O_{12}$ substrate was observed due to the volatility of gallium oxide Ga_2O. This leads to the formation of a surface layer of $Gd_3(Fe_xGa_{5-x})O_{12}$ in the substrate, which occurred as a result of filling vacancies formed during partial loss of gallium with Fe^{3+} ions. It is obvious that vacancies $V_{Ga}^{¢¢¢}$, occupied by iron ions, were formed primarily in octahedral positions. The diffraction peak **2** in Fig. 3 indicates the formation of the epitaxial layer of $Gd_3(Fe_xGa_{5-x})O_{12}$. The calculated unit cell parameter for the $Gd_3(Fe_xGa_{5-x})O_{12}$ layer was 12.46 Å, which was close to the unit cell parameter for $Gd_3Fe_5O_{12}$ = 12.50 Å.

Diffraction peak **3** (Fig. 3a, b) we interpret as belonging to the intermediate Tm-excessive layer of garnet of composition $Tm_3(Tm_xFe_{5-x})O_{12}$, similar to $Lu_3(Lu_xFe_{5-x})O_{12}$, observed in [14] and formed as a result of partial occupation of octahedral positions of garnet by Lu^{+3} ions and a decrease in their occupation by Fe^{+3} ions. Since the ionic radius of Tm^{+3} (coordination number = 6) is higher than that of Fe^{+3} (0.88 Å and 0.65 Å, respectively [15]), then such a substitution leads to a strong increase in the unit cell parameter of the Tm^{+3} compositions as the x value increases, which is manifested in a shift in the X-ray reflection of garnet (444) to the region of smaller angles. The possibility of the location of REE ions not only in dodecahedral but also in octahedral positions was pointed out by Geller in his classic study in 1967 on the crystallography of garnets [6]. Also the theoretical study[16], which examined these possibilities in detail and proposes an algorithm for calculating the degree of occupation of oxygen octahedra in garnet single crystals by REE ions, as well as the study [17], in which the formation of such antisite defects in a number of garnets, studied by the EXAFS method, was considered as the cause of a decrease in the cubic symmetry of garnets should be mentioned. At the same time, systematic and convincing experimental evidence of such a redistribution of REE ions by positions, as well as reliably established information about the region of non-stoichiometry of garnets in the systems "REE oxide – A_2O_3 (A = Al, Ga, Fe)" could not be found in the literature. In addition, it should be noted that the possibility of formation of antisite defects $[RE_{Fe}]^{3+}$ in heteroepitaxial films and autonomous phases (powders, single crystals)

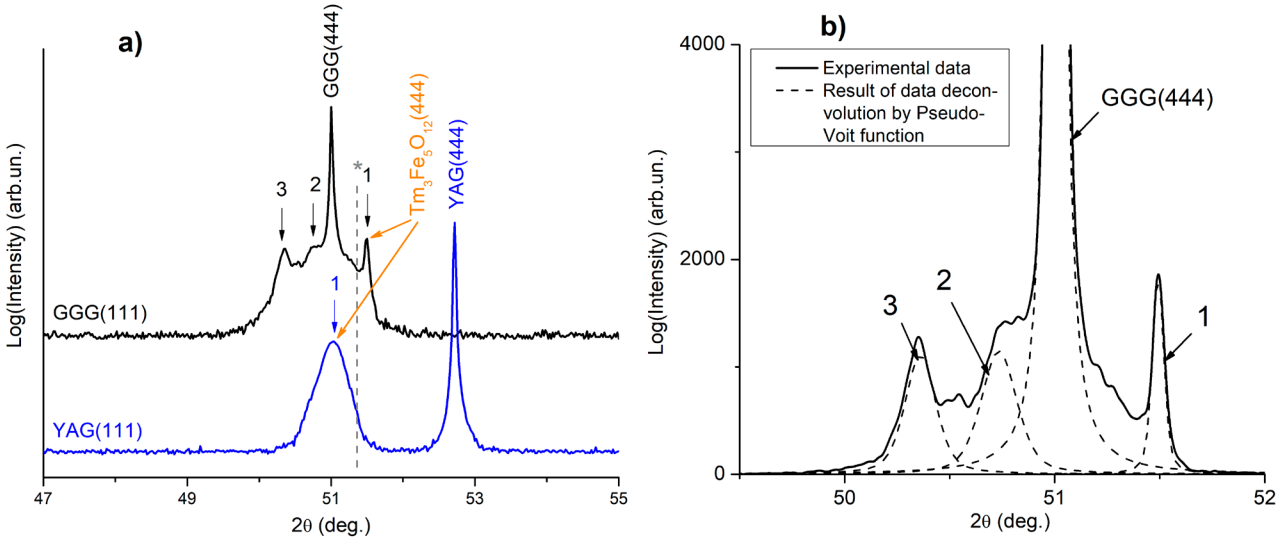

Fig. 3. (a) X-ray diffractograms of $Tm_3Fe_5O_{12}$ films deposited on GGG(111) and YAG(111) substrates. The dashed line indicates the (444) peak position of bulk $Tm_3Fe_5O_{12}$. (b) Magnified fragment of the diffractogram of $Tm_3Fe_5O_{12}$ film deposited on GGG(111) with description of the pseudo-Voit function of the film peaks (peaks **1**–**3**) and the substrate peak

of the same composition, can differ significantly, since the films in the immediate vicinity of the interface with the substrate are always strained (in-plane tensile or compressive strain), which can, depending on the sign of the deformation, promote or counteract the formation of films enriched in REE, with an increased parameter in the plane of the interface. During the growth of $Tm_3Fe_5O_{12}$ on GGG a positive ε value, which means the in-plane tensile of the film, can lead to the growth of the film with an increased unit cell parameter, i.e. contribute to the formation of antisite defects $[RE_{Fe}]^{3+}$ and the formation of a layer of Tm-enriched garnet.

Based on the established sequence of growth of the interface layers, it is possible to assume a common cause and diffusion mechanism for their occurrence: the removal of gallium from the surface layer of the substrate causes a counter diffusion flow of iron ions into the substrate from the adjacent thin layer of stoichiometric $Tm_3Fe_5O_{12}$ garnet which leads to enrichment of the latter with a rare earth component. It should be noted that both interface layers have a garnet structure and therefore do not impair the epitaxial character and orientation of the deposited layer, considered at full thickness. Epitaxial nature of $Tm_3Fe_5O_{12}$ films on GGG(111) and YAG(111) substrates was confirmed by X-ray φ-scanning (Fig. 4a, b): since the position of the reflections (800) of the film and substrate on the φ-scans coincided, it can be concluded that during $Tm_3Fe_5O_{12}$/GGG(111) and $Tm_3Fe_5O_{12}$/YAG(111) film growth, cube-on-cube heteroepitaxy occurs.

Garnet of the "correct stoichiometry" 3:5 on the diffraction pattern of the $Tm_3Fe_5O_{12}$/GGG sample corresponds to the peak number **1** (Fig. 3a, b). It corresponds to the reflection from the (444) plane, and its position corresponds to that expected based on the powder diffraction pattern (the position of the $Tm_3Fe_5O_{12}$(444) peak for the powder is indicated by a dashed line) taking into account the above-described nature of epitaxial deformations: in-plane tensile strain)and the resulting reduction in interplanar distances in the direction perpendicular to the substrate (out-of-plane). The fact that the deviation of the (444) reflex from the line for the powder is relatively small indicates a small amount of film deformation during heteroepitaxy on a substrate with a very different unit cell parameter. In accordance with theoretical concepts of heteroepitaxy [18], partial elimination of elastic stresses arising due to the parametric difference between the film and the substrate occurs in this case due to the emergence of misfit dislocations (MD) in the film. It is natural to assume that in this case the MD are formed at the boundary of the Tm-excess layer of $Tm_3(Tm_xFe_{5-x})O_{12}$ and stoichiometric layer $Tm_3Fe_5O_{12}$, which differ most significantly by the unit cell parameter.

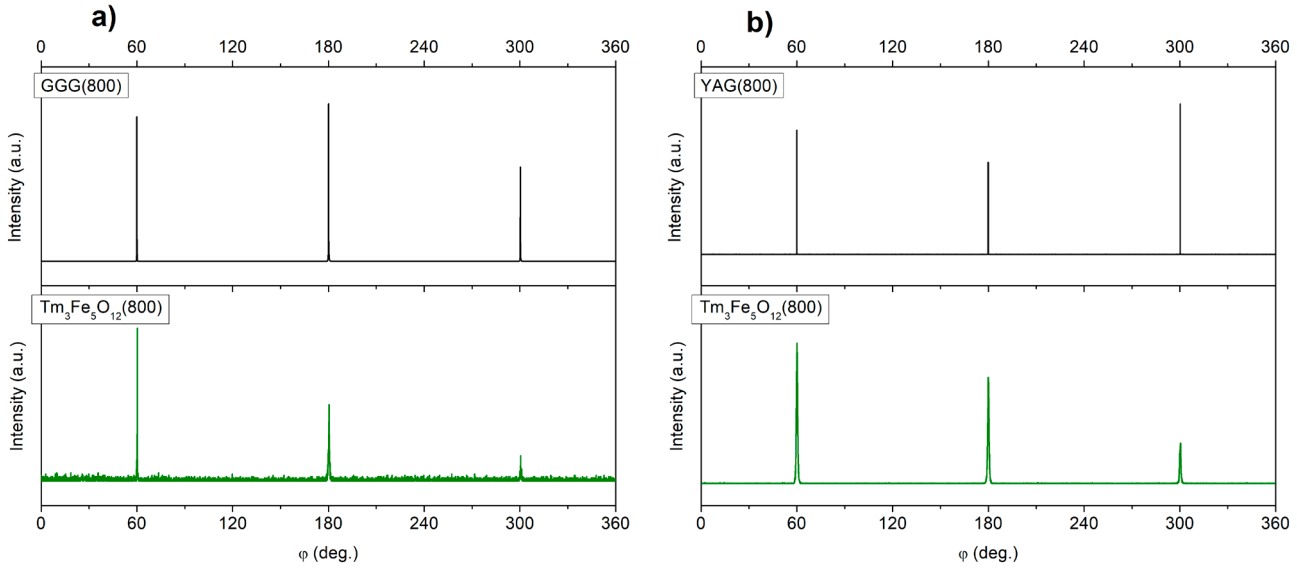

Fig. 4. X-ray φ-scans results for $Tm_3Fe_5O_{12}$ films on GGG(111) (a) and YAG(111) (b) substrates

As the result of the deposition of $Tm_3Fe_5O_{12}$ films on a YAG(111) substrate, which has a lower unit cell parameter than the film and a larger parametric mismatch, was the formation of highly strained film, as indicated by the large deviation of the (444) reflex from its position for the powder sample (Fig. 3a). In this case, the stress is of compressive nature along the substrate, which, in accordance with the elastic nature of the deformation, led to stretching of the film along the normal to the substrate (as was indicated by the shift of the film peak towards smaller angles relative to the peak for the powder). Strong elastic strains in the film were manifested not only as a large shift of the (444) reflex, but also as its significant broadening: the width at half maximum (FWHM) was 0.31°. The magnitude of elastic strains s is of interest. The value of s was calculated based on the relative change of unit cell parameter of the film's e compared to a $Tm_3Fe_5O_{12}$ single crystal using the ratios:

$$\varepsilon = \frac{a_{film} - a_{Tm_3Fe_5O_{12}}}{a_{Tm_3Fe_5O_{12}}}, \quad (6)$$

$$\sigma = \frac{E}{1-\nu}\varepsilon, \quad (7)$$

where a_{film} = 12.391 Å (the unit cell parameter determined based on XRD data for the $Tm_3Fe_5O_{12}$ film) and $a_{Tm_3Fe_5O_{12}}$ = 12.327 Å (the unit cell parameter for the $Tm_3Fe_5O_{12}$ single crystal), E – Young's modulus, ν – Poisson's ratio. Since the elastic constants for $Tm_3Fe_5O_{12}$ are not available in the literature, we used E = 187 GPa and ν = 0.29 for yttrium iron garnet $Y_3Fe_5O_{12}$ for the calculation [19]. The compressive stresses determined in this way was 1.4 GPa. It is obvious that, despite its large value, the compressive stresses characterizes only the stress remaining after part of it has been eliminated by the appearance of MD at the film/substrate interface. The value of the theoretically possible elastic stress arising in the absence of the dislocation relaxation mechanism was estimated according to the formula:

$$\sigma = \frac{E}{1-\nu} \cdot \frac{a_{Tm_3Fe_5O_{12}} - a_{YAG}}{a_{YAG}} \quad (8)$$

and composed ~7 GPA (a_{YAG} = 12.010 Å). Thus it becomes clear that the elastic stresses at the interface $Tm_3Fe_5O_{12}$ with YAG substrate by» 80% are eliminated by mismatch dislocations.

In conclusion of the discussion of the X-ray diffraction results, it is necessary to state the degradation of $Gd_3Ga_5O_{12}$-based substrates during gas-phase deposition, which led to the formation of additional phases in the composition of the $Tm_3Fe_5O_{12}$ film and to the impossibility of using GGG(111) substrates to obtain iron garnet films for applied research, including for studying their behavior in the terahertz region. In this regard, YAG substrates, which are quite stable under high-temperature conditions of film deposition using vacuum methods, despite the greater parametric mismatch, show a significant advantage.

The Raman scattering studies of synthesized $Tm_3Fe_5O_{12}$/YAG(111) film and YAG substrates were conducted at wavelengths λ = 532 nm (Fig. 5a) and λ = 785 nm (Fig. 5b). The iron garnets belong to the space group *Ia*3*d* and according to [20] have the following set of vibrational modes:

$$\Gamma = 3A_{1g} + 6E_g + 9T_{2g} + 9T_{1u}. \quad (1)$$

The YAG belongs to the same space group, and as studies of the YAG structure have shown [21], yttrium ions have 24 c-bonds with dodecahedral coordination, and aluminum ions have 16 a-bonds with octahedral coordination and 24 d-bonds with tetrahedral oxygen coordination. These 160 atoms (metals and oxygen) per unit cell create 18 phonon branches (17 optical and 1 acoustic T_{1u}). It should be noted that 18 Raman-active modes A_{1g}, E_g and T_{2g}, and 9 IR-active oscillations T_{1u} are possible for the space group *Ia*3*d* [22].

Our Raman study showed that the best resolution of vibrational modes of the $Tm_3Fe_5O_{12}$ film against the background of a single-crystal YAG substrate was observed at λ = 532 nm (Fig. 5a): the spectrum allows modes at 117 (T_{2g}), 182, 469, 650, 1114, 1284, 1817, 1910 and 1960 cm^{-1}. With less energy irradiation with a longer wavelength λ = 785 nm, weak differences were observed between the spectrum of the YAG substrate and the spectrum of the film (Fig. 5b): only 2 vibrational modes were allowed at 116 (T_{2g}) and 251 cm 1 (E_{2g}). This is due to the fact that with a decrease in wavelength, starting from 800 nm, the absorption of rare earth iron garnets increases significantly. This, in turn, was associated with intense interband transitions and charge transfer

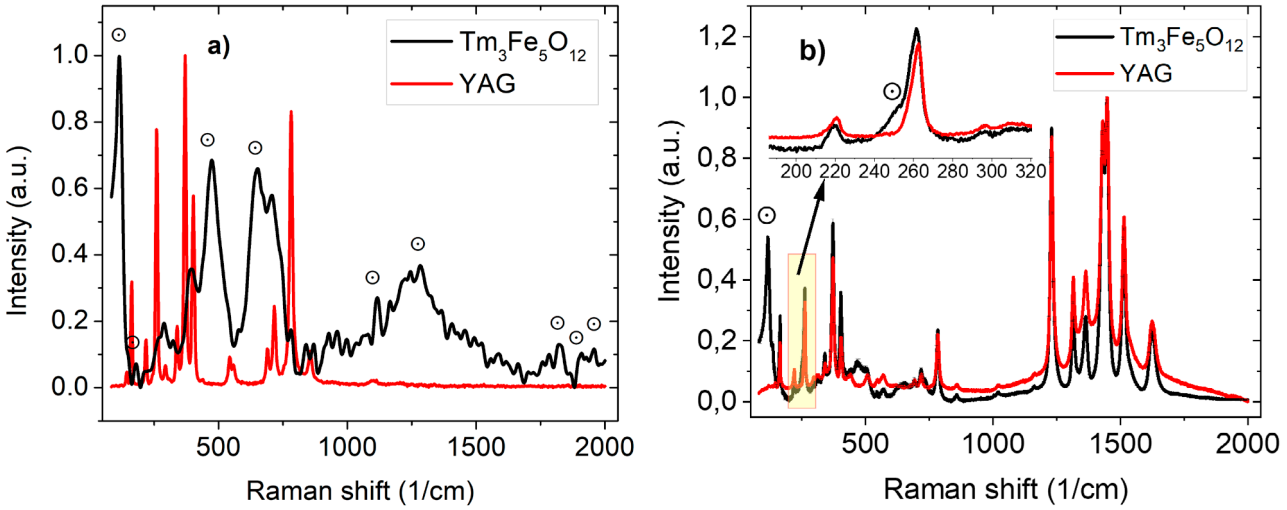

Fig. 5. Raman spectra of $Tm_3Fe_5O_{12}$ film on YAG(111) substrate at wavelengths of 532 nm (a) and 785 nm (b). ⊙ – vibrational modes related to the $Tm_3Fe_5O_{12}$ film

transitions from O^{2-} to Fe^{3+} or to the rare earth element ion RE^{3+} [23]. The obtained Raman shifts 116 and 251 cm^{-1} were consistent with the data for $Tm_3Fe_5O_{12}$ films with the thickness of 20–300 nm on a substituted gallium-gadolinium garnet ($Gd_{2.6}Ca_{0.4}Ga_{4.1}Mg_{0.25}Zr_{0.65}O_{12}$) substrate with orientation (111), in the Raman spectra of which 2 modes were observed – 130 and 250 cm^{-1} when shooting up to 300 cm^{-1} was performed [24].

The study [22] demonstrated that Raman spectra have a relatively low signal-to-noise ratio at frequencies below a few terahertz (150 cm^{-1}). In this regard, as another method of vibrational spectroscopy, we performed THz-pulse spectroscopy, which allows restoring the dielectric characteristics of various materials in the frequency range from 0.1 to 10 Thz. In this study, the dielectric characteristics of GGG and YAG substrates (with thicknesses of 513 μm and 502 μm, respectively) were investigated based on measurements of THz radiation transmission (Fig. 6). These measurements also indicate that the YAG(111) substrate is more promising than the GGG(111) substrate, since its characteristic spectrum does not show significant absorption in a wider frequency range from 0.25 to 3.0 THz, while GGG substrates have an absorption line at a frequency of 2.5 THz, which reduces the spectral range for film analysis to 0.2–2.2 THz. Thus, despite the stressed nature of the $Tm_3Fe_5O_{12}$ films, obtained on a YAG(111) substrate, such films appear more promising for further terahertz research. A resonant absorption mode was detected for the YAG(111) substrate at a frequency of 3.25 THz (108 cm^{-1}). The observed resonant absorption mode can be explained by a two-phonon difference process, as a result of which an acoustic phonon is transferred to the optical branch [22].

Due to the low film thickness compared to the wavelength of THz radiation, we simultaneously measure THz fields reflected and transmitted through the $Tm_3Fe_5O_{12}$ film on the YAG substrate. This approach improves the accuracy of the reconstruction of THz characteristics of thin films [25, 26]. The transmittance/reflectance spectra of the YAG(111) substrate and $Tm_3Fe_5O_{12}$ film on

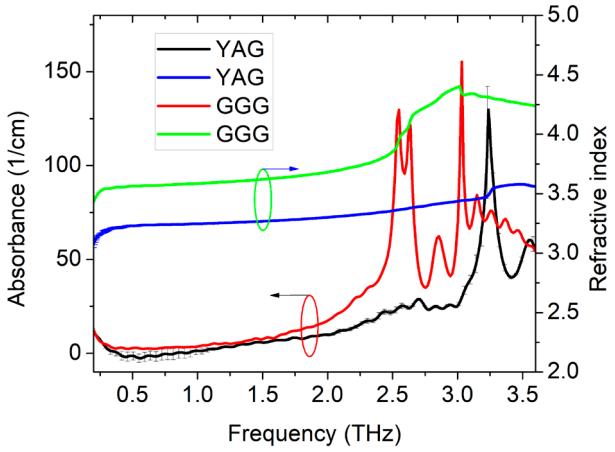

Fig. 6. Absorption coefficient and refractive index spectra of GGG(111) and YAG(111) substrates in the frequency range from 0.2 to 3.6 THz

this substrate are shown in Fig. 7a. As a result of the reconstruction of the THz characteristics [26], the spectra of the absorption coefficient and refractive index of the thulium iron garnet film on the YAG substrate were obtained (see Fig. 7b). The absorption coefficient tends to increase slowly in the high frequency region. The refractive index of the film has a large dispersion. At a fixed frequency of 2 THz, the absorption coefficient of the film was 13 cm^{-1}, and the refractive index was 2.8, which is typical for materials with low conductivity.

4. Conclusions

Thin $Tm_3Fe_5O_{12}$ iron garnet films were obtained on single-crystal GGG(111) and YAG(111) substrates using the MOCVD method. It was found that due to the volatility of gallium(I) oxide under deposition conditions (910 °C and P_{O2} = 1 mbar) the introduction of iron oxide into the surface layer of the substrate and enrichment of the adjacent layer of the film with thulium oxide occurs, which leads to the formation of non-stoichiometric garnet $Tm_3(Tm_xFe_{5-x})O_{12}$ with antisite defects [Tm_{Fe}^{3+}]. Thus, the epitaxial film of stoichiometric garnet $Tm_3Fe_5O_{12}$ grows on a GGG substrate with two interface layers. On the YAG substrate, the thulium iron garnet film is deposited without chemical interaction at the interface, but experiences strong in-plane compressive stress from the substrate. Films on a YAG substrate, transparent up to a frequency of 3.5 THz, have an advantage over films on GGG from the point of view of potential application in THz-range technology. As a result of the reconstruction of the THz characteristics, the frequency dependences of the absorption coefficient and the refractive index of the $Tm_3Fe_5O_{12}$ film on a YAG substrate were obtained.

Author contributions

Markelova M. N. – scientific supervision, research concept, processing of X-ray diffraction results and text writing. Hafizov A. A., Shi X. – conducting experiments on gas-phase deposition of thin films, processing the results of X-ray diffraction. Graboy I. E. – development of methodology, text writing. Shanin M. S., Konnikova M. R. – conducting experiments on Raman spectroscopy and terahertz spectroscopy. Shkurinov A. P. – scientific supervision, research concept, methodology development. Kaul A. R. – scientific supervision, research concept, methodology development, text editing.

Conflict of interests

The authors declare that they have no known competing financial interests or personal relationships that could have influenced the work reported in this paper.

References

1. Nikitov S. A., Kalyabin D. V., Lisenkov I. V. ... Pavlov E. S. Magnonics: a new research area in spintronics

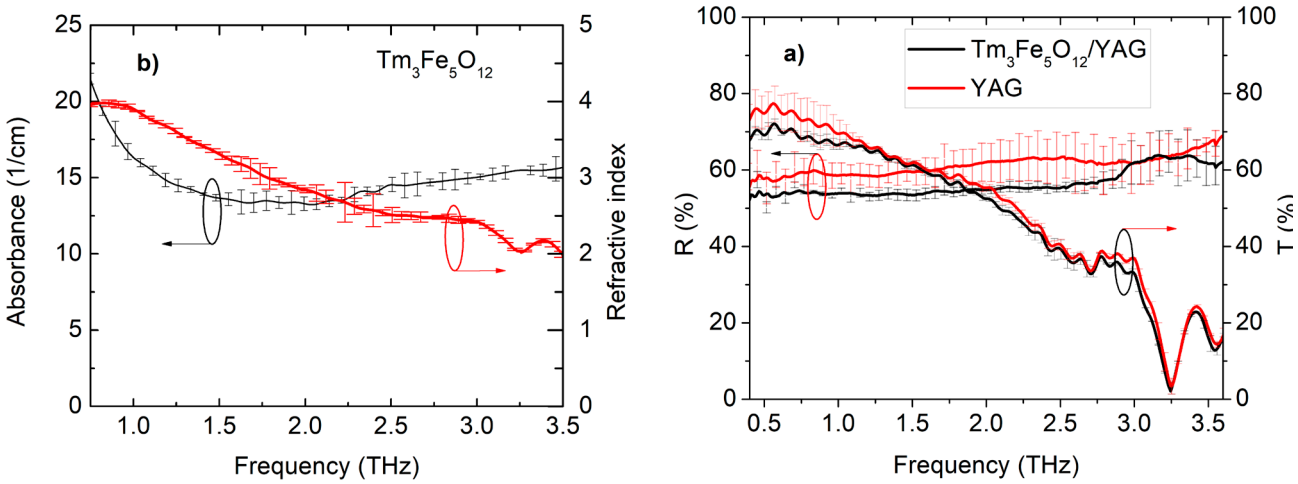

Fig. 7. Transmission, reflection (a), absorption and refractive index spectra of $Tm_3Fe_5O_{12}$ film (b) on YAG substrate in the THz frequency range. The standard deviation is calculated for three independent averages of 1000 accumulations each

and spin wave electronics. *Physics-Uspekhi*. 2015;58: 1002–1028. https://doi.org/10.3367/UFNr.0185.201510m.1099

2. Robertson J. M. Liquid phase epitaxy of garnets. *Journal of Crystal Growth*. 1978;45: 233–242. https://doi.org/10.1016/0022-0248(78)90441-4

3. Hibiya, T., Görnert, P. *Liquid phase epitaxy of garnets. Liquid phase epitaxy of electronic, optical and optoelectronic materials*. P. Capper and M. Mauk (eds.). John Wiley & Sons Limited, US; 2007. p. 305–339. https://doi.org/10.1002/9780470319505.ch11

4. Akchurin R. H., Marmalyuk A. A. *MOC-hydrid epitaxy in the technology of materials for photonics and electronics**. Technosphera Publ.; 2018. 488 p. (In Russ.)

5. Kaul A. R., Gorbenko O. Yu., Kamenev A. A. The role of heteroepitaxy in the development of new thin-film oxide-based functional materials. *Russian Chemical Reviews*. 2004;73(9): 861–880. https://doi.org/10.1070/rc2004v073n09abeh000919

6. Geller S. Crystal chemistry of the garnets. *Zeitschrift für Kristallographie*; 1967;125: 1–47. https://doi.org/10.1524/zkri.1967.125.16.1

7. Blank T. G. H., Mashkovich E. A., Grishunin K. A., ... Kimel A. V. Effective rectification of terahertz electromagnetic fields in a ferrimagnetic iron garnet. *Physical Review B* 2023;108: 094439. https://doi.org/10.1103/PhysRevB.108.094439

8. Volkov D. A., Gabrielyan D. A., Matveev A. A., ... Nikitov S. A. Spin pumping from $Lu_3Fe_5O_{12}$. *JETP Letters*. 2024;119(5): 357–362. https://doi.org/10.1134/S0021364024600150

9. Kudasov Yu. B., Logunov M. V., Kozabaranov R. V., ... Svetlov A. S. Magnetooptic properties of bismuth-substituted ferrite–garnet films in strong pulsed magnetic fields. *Physics of the Solid State*; 2018;60(11): 2207–2210. https://doi.org/10.1134/S106378341811015X

10. Kirilyuk A., Kimel A. V., Rasing T. Ultrafast optical manipulation of magnetic order. *Reviews of Modern Physics*. 2016;88: 039904. https://doi.org/10.1103/RevModPhys.82.2731

11. Kaul A. R., Nygaard R. R., Ratovskiy V. Yu., Vasiliev A. L. TSF-MOCVD – a novel technique for chemical vapour deposition on oxide thin films and layered heterostructures. *Kondensirovannye sredy i mezhfaznye granitsy = Condensed Matter and Interphases*. 2021;23(3): 396–405. https://doi.org/10.17308/kcmf.2021.23/3531

12. Nazarov M. M., Makarova S. A., Shkurinov A. P., Okhotnikov O. G. The use of combination of nonlinear optical materials to control terahertz pulse generation and detection. *Applied Physics Letters.* 2008;92: 021114. https://doi.org/10.1063/1.2831658

13. Coutaz J.-L., Garet F., Wallace V. *Principles of terahertz time-domain spectroscopy*. (1st ed.). New York: Jenny Stanford Publishing; 2018. 640 p. https://doi.org/10.1201/b22478

14. Hafizov A. A., Markelova M. N., Gu R., ... Kaul A. R. Gas-phase deposition, structure and ferrimagnetic resonance of epitaxial garnet films of $Lu_3Fe_5O_{12}$*. *Solid state chemistry and functional materials – 2024: Proc. XIII All-Russ. Conf., 16–20 September 2024.* St. Petersburg: Novbytkhim Publ.; 2024. p. 405. (In Russ.)

15. Shannon R. D. Revised effective ionic radii and systematic studies of interatomic distances in halides and chalcogenides. *Acta Crystallographica Section A*. 1976;A32: 751–767. https://doi.org/10.1107/S0567739476001551

16. Karban' O. V. *Defects, crystal ordering, properties of oxides with garnet structure**. Cand. Phys. and Math. diss. Abstr. Izhevsk: 1999. 169 p. (In Russ.). Available at: https://www.dissercat.com/content/defekty-kristallograficheskoe-uporyadochenie-svoistva-oksidov-so-strukturoi-granata

17. Dong J., Lu K. Non-cubic symmetry in garnet structures studied using extended x-ray absorption fine-structure spectra. *Physical Review B*. 1999;43(11): 8808–8821. https://doi.org/10.1103/PhysRevB.43.8808

18. Efimov A. N., Lebedev A. O. *Geometric aspects of heteroepitaxy**. St. Petersburg: SPbGETU «LETI» Publ.; 2012. 110 p. (In Russ.)

19. Rabkin L. I., Soskin S. A., Epshtein B. Sh. *Ferrites. Structure, properties, production technology**. Leningrad: Energy Publ.; 1968. 384 p. (In Russ.)

20. Bilbao Crystallographic Server. Available at: https://www.cryst.ehu.es/

21. McDevitt N. T. Infrared lattice spectra of rare-earth aluminum, gallium, and iron garnets. *Journal of the Optical Society of America*. 1969;59(9): 1240–1244. https://doi.org/10.1364/josa.59.001240

22. Gaume R., Steere D., Sundaram S. K. Effect of nonstoichiometry on the terahertz absorption of $Y_3Al_5O_{12}$ optical ceramics. *Journal of Materials Research*. 2014;29(19): 2338–2343. https://doi.org/10.1557/jmr.2014.236

23. Pavlov V. V., Pisarev R. V., Fiebig M., Fröhlich D. Optical harmonic generation in magnetic garnet epitaxial films near the fundamental absorption edge. *Physics of the Solid State*; 2003:45(4): 662–669. https://doi.org/10.1134/1.1569002

24. Sharma A., Ciubotariu O. T., Matthes P., ... Salvan G. Optical and magneto-optical properties of pulsed laser-deposited thulium iron garnet thin films. *Applied Research*. 2024;3: e202200064. https://doi.org/10.1002/appl.202200064

25. Konnikova M. R., Tretyakov A. K., Shevchenko A. R., ... Shkurinov A. P. PCM for driving active THz modulators: frequency and polarization sensitivity. *2024 International Conference Laser Optics (ICLO)*, Saint Petersburg, Russian Federation, 2024: c. 326–326. https://doi.org/10.1109/ICLO59702.2024.10624176

26. Konnikova M., Tretyakov A., Kistenev Y., Ozheredov I., Coutaz J.-L., Shkurinov A. Novel method for extracting electromagnetic parameters of thin films based on dual-mode terahertz time-domain spectroscopy measurements. *Journal of Infrared, Millimeter, and Terahertz Waves*; 2024. (in press)

** Translated by author of the article*

Information about the authors

Maria N. Markelova, Cand. Sci. (Chem.), Research Fellow at the Department of Chemistry, Lomonosov Moscow State University (Moscow, Russian Federation).
https://orcid.org/0000-0002-1014-9437
maria.markelova@gmail.com

Abduvosit A. Hafizov, graduate student at the Higher School of Material Science, Lomonosov Moscow State University (Moscow, Russian Federation).
https://orcid.org/0009-0003-0740-8180
abduvosithafizov220@gmail.com

Xiaoyu Shi, master degree student at the Higher School of Material Science, Lomonosov Moscow State University (Moscow, Russian Federation).
https://orcid.org/0009-0007-4025-9032
s1169608828@gmail.com

Igor E. Graboy, Cand. Sci. (Chem.), Senior Research Fellow at the Department of Chemistry, Lomonosov Moscow State University (Moscow, Russian Federation).
https://orcid.org/0009-0003-7011-2200
graboi@inorg.chem.msu.ru

Maxim S. Shanin, graduate student, Junior Research Fellow at the Department of Physics, Lomonosov Moscow State University (Moscow, Russian Federation); Research Fellow at National Research Centre "Kurchatov Institute" (Moscow, Russian Federation).
https://orcid.org/0009-0007-7215-4024
shaninms@my.msu.ru

Maria R. Konnikova, Junior Research Fellow at the Department of Physics, Lomonosov Moscow State University (Moscow, Russian Federation); Junior Research Fellow at National Research Centre "Kurchatov Institute" (Moscow, Russian Federation).
https://orcid.org/0000-0003-4701-6483
konnikova.mr20@physics.msu.ru

Alexander P. Shkurinov , Dr. Sci. (Phys.–Math.), Corresponding member of the Russian Academy of Sciences, Full Professor at the Chair of General Physics and Wave Processes, Lomonosov Moscow State University (Moscow, Russian Federation).
https://orcid.org/0000-0002-6309-4732
ashkurinov@physics.msu.ru

Andrey R. Kaul, Dr. Sci. (Chem.), Full Professor at the Chair of Inorganic Chemistry, Lomonosov Moscow State University, Moscow, Russian Federation
https://orcid.org/0000-0002-3582-3467
arkaul@mail.ru

Received 14.08.2024; approved after reviewing 10.09.2024; accepted for publication 16.09.2024; published online 25.03.2025.

Translation by Valentina Mittova